Radiology

Pari V. Pandharipande, MD
Glenn A. Krinsky, MD
Henry Rusinek, PhD
Vivian S. Lee, MD, PhD

**Published online**
10.1148/radiol.2343031362
**Radiology 2005;** 234:661–673

**Abbreviation:**
HCC = hepatocellular carcinoma

[1] From the MRI-Basement, Schwartz Bldg, NYU Medical Center, 530 First Ave, New York, NY 10016. Received August 25, 2003; revision requested November 6; revision received February 3, 2004; accepted March 23. **Address correspondence to** V.S.L. (e-mail: *vivian.lee@med.nyu.edu*).

V.S.L. is on the Speakers' Bureau for Berlex Laboratories.



# Perfusion Imaging of the Liver: Current Challenges and Future Goals[1]

Improved therapeutic options for hepatocellular carcinoma and metastatic disease place greater demands on diagnostic and surveillance tests for liver disease. Existing diagnostic imaging techniques provide limited evaluation of tissue characteristics beyond morphology; perfusion imaging of the liver has potential to improve this shortcoming. The ability to resolve hepatic arterial and portal venous components of blood flow on a global and regional basis constitutes the primary goal of liver perfusion imaging. Earlier detection of primary and metastatic hepatic malignancies and cirrhosis may be possible on the basis of relative increases in hepatic arterial blood flow associated with these diseases. To date, liver flow scintigraphy and flow quantification at Doppler ultrasonography have focused on characterization of global abnormalities. Computed tomography (CT) and magnetic resonance (MR) imaging can provide regional and global parameters, a critical goal for tumor surveillance. Several challenges remain: reduced radiation doses associated with CT perfusion imaging, improved spatial and temporal resolution at MR imaging, accurate quantification of tissue contrast material at MR imaging, and validation of parameters obtained from fitting enhancement curves to biokinetic models, applicable to all perfusion methods. Continued progress in this new field of liver imaging may have profound implications for large patient groups at risk for liver disease.


Perfusion imaging provides the ability to detect regional and global alterations in organ blood flow. The utility of hepatic perfusion characterization relies on the resolution of each component of its dual blood supply—the portal vein and the hepatic artery—because contributions from each are altered predictably in many diseases. As early as 1954, Breedis and Young (1) first described relative increases in arterial supply in the setting of primary and metastatic liver tumors, thus heralding the possibility of arterial phase imaging to detect malignant tumors. Changes in relative arterial and portal venous blood flow also are known to be associated with the evolution of cirrhosis (2,3). Because most pathologic entities of the liver affect blood flow regionally, globally, or both (4), perfusion imaging of the liver has been invoked as a means of improving the sensitivity and specificity of diagnostic liver imaging. Herein, we provide a context for liver perfusion imaging and review its physiologic basis. After highlighting goals for its use and development, we review existing methods and discuss their role in the evaluation of cirrhosis, hepatocellular carcinoma (HCC), and metastatic disease. We conclude with a consideration of future directions in this emerging field.

## BACKGROUND: NEED FOR IMPROVED LIVER IMAGING

To date, existing imaging methods for the diagnosis of cirrhosis and HCC are falling short of clinical needs. For the detection of cirrhosis, imaging techniques rely primarily on morphologic criteria—particularly identification of a nodular liver surface and liver atrophy with secondary signs of portal hypertension. Ultrasonography (US) has been reported to have a sensitivity of 74% (79 of 107 patients) (5) to 88% (50 of 57 patients) (6) for the detection of cirrhosis (5–7) when liver biopsy and/or gross observation at laparoscopy were used as standards of reference. Multiphasic contrast material–enhanced CT protocols have

## ESSENTIALS

- *Improved therapeutic options for hepatocellular carcinoma and metastatic disease have placed greater demands on liver imaging.*
- *Existing diagnostic imaging techniques provide limited evaluation of tissue characteristics beyond morphology; liver perfusion imaging has the potential to improve this shortcoming.*
- *The primary goal of perfusion imaging of the liver is to enable resolution of arterial and portal venous components of blood flow on a global and regional basis.*
- *Earlier detection of primary and metastatic hepatic malignancies and cirrhosis may be possible on the basis of relative increases in hepatic arterial blood flow in these diseases.*
- *While several technical challenges remain, continued progress in this new field of liver imaging may have profound implications for the diagnosis and surveillance of liver diseases in the future.*

been reported to have sensitivities of 6% (two of 33 lesions) (8) to 71% (15 of 21 lesions) (9) for the detection of HCC and 0% (zero of 22 lesions) (10) to 39% (nine of 23 lesions) (9) for the detection of dysplastic nodules, which are premalignant precursors of HCC (8–12), when liver explant abnormalities are used as a standard of reference. With multiphasic contrast-enhanced MR imaging, sensitivity values of 33% (39 of 118 lesions) (13) to 76.9% (10 of 13 lesions) (12) have been reported for HCC detection and 7% (one of 15 lesions) (13) to 56% (22 of 39 lesions) (8) for dysplastic nodule detection (8,10,12–14) when liver explant abnormalities were used as a standard of reference. In two studies in which lesions were stratified by size, however, sensitivity values for detection of HCC smaller than 1 cm were 4% (three of 72 lesions) (13) and 26.7% (four of 15 lesions) (10). In addition, in one study of nine patients who had diffuse HCC (all nodules $< 1$ cm), only three lesions (all from one patient) were detected (13).

From a public health perspective, the potential benefit of higher sensitivity and higher specificity liver imaging has increased substantially in recent years. HCC, the most common primary liver cancer and fifth most common cancer in the world, is responsible for more than one-half million deaths annually worldwide (15). While the reported 3-year survival rate for untreated small HCC ($\leq$5 cm) is 21% (16), the 4-year survival rate in patients with cirrhosis who undergo transplantation for small HCC (one lesion of $\leq$5 cm or as many as three lesions of $\leq$3 cm) is approximately 75% (17). This discrepancy suggests that early detection of small HCC may be critical to patient outcome. Greater organ availability made possible by the increasing practice of adult-to-adult living related liver donor transplantation (18), combined with improved detection of small HCC, has the potential to dramatically influence the care of patients at risk. The early noninvasive detection of cirrhosis may enable earlier identification of patients at risk for HCC and more timely treatment of the diseases that cause cirrhosis; moreover, noninvasive detection may obviate histologic sampling.

For the evaluation of metastatic disease, sensitivity values of 74% (60 of 81 metastases) (19) to 85% (247 of 290 metastases) (20) have been reported when contrast-enhanced CT is used (19–21); in the study by Ward et al (19), 17 metastases missed by all readers were smaller than 1 cm. Histologic evaluation of surgical specimens, as well as intraoperative US and gross examination of the unresected liver, were used as standards of reference (19–21). Improved detection and characterization of metastatic disease to the liver also has profound implications for the prognosis and treatment of patients at risk. The earlier identification of patients with micrometastatic disease may facilitate future use of targeted chemotherapeutic strategies. Antiangiogenic therapies targeted against vascular endothelial growth factors already have demonstrated promising results for the treatment of multiple cancers in phase II clinical trials (22,23). Moreover, exclusion of the presence of micrometastatic disease could obviate adjuvant chemotherapy in some patient groups. Improved detection of focal metastatic disease also may affect the outcome in candidates for segmental hepatectomy (24–28).

## PERFUSION IMAGING OF THE LIVER: PHYSIOLOGIC AND STRUCTURAL BASIS

### Normal Liver Anatomy: Brief Review

In the normal liver, approximately three-quarters of the blood supply is derived from the portal vein, whereas only about one-quarter is derived from the hepatic artery (29,30). The organization and delivery of this blood supply is best understood by first observing the underlying structure of the liver.

The liver is organized into small units called acini, which consist of a central incoming blood supply from hepatic arterial and portal venous branches, bile ducts, cords of liver cells, intervening sinusoids, and a peripheral outgoing systemic venous blood supply (Fig 1). The low-pressure sinusoids are lined with highly fenestrated endothelial cells and are flanked by sheets of hepatocytes. This arrangement allows plasma to flow freely through the sinusoidal endothelial cells into the space between sinusoidal endothelium and hepatocytes; this space is termed the *space of Disse* (Fig 2). Low-molecular-weight compounds within serum plasma, including conventional contrast materials, typically have free access to the space of Disse.

### Evolution of Cirrhosis

The evolution of cirrhosis is associated with a progressive disruption of normal anatomy and physiology, which leads to both regional and global perfusion changes. Deposition of collagen in the space of Disse and alteration of sinusoidal architecture through the loss of fenestra between sinusoidal endothelial cells together result in an increase in resistance to incoming sinusoidal blood flow. As a result, portal venous flow decreases and begins to bypass the liver parenchyma via small portosystemic venous shunts. The mean transit time, a parameter defined as the traversal time of a compound from liver entry to exit averaged over all possible paths, of low-molecular-weight compounds through the liver is increased. This increase is attributed to restriction of movement within the extravascular space caused by deposition of collagen (31,32). In cirrhosis, this alteration of portal venous blood flow is counteracted by an increase in hepatic arterial flow, a process known as the hepatic arterial buffer response (2,3). By studying different markers of liver function (such as lidocaine metabolism)

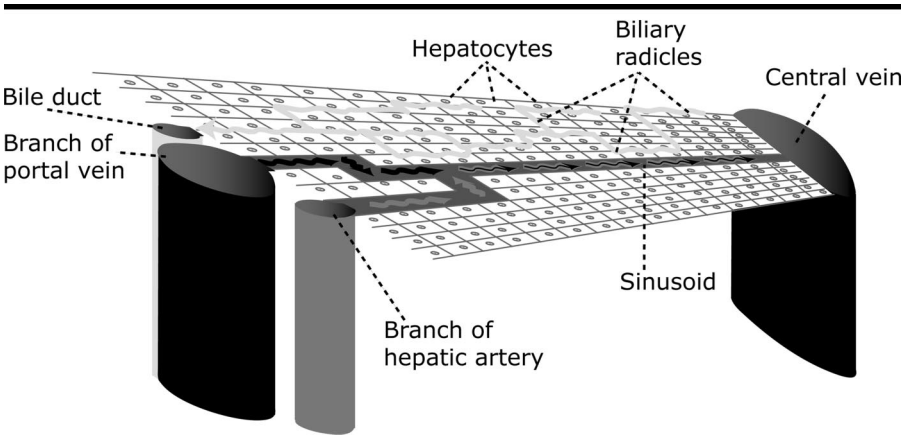


**Figure 1.** Diagram shows anatomic relationship between hepatic arterial and portal venous branches and bile duct (portal triad), biliary radicles, cords of hepatocytes, intervening sinusoid, and central draining hepatic vein.

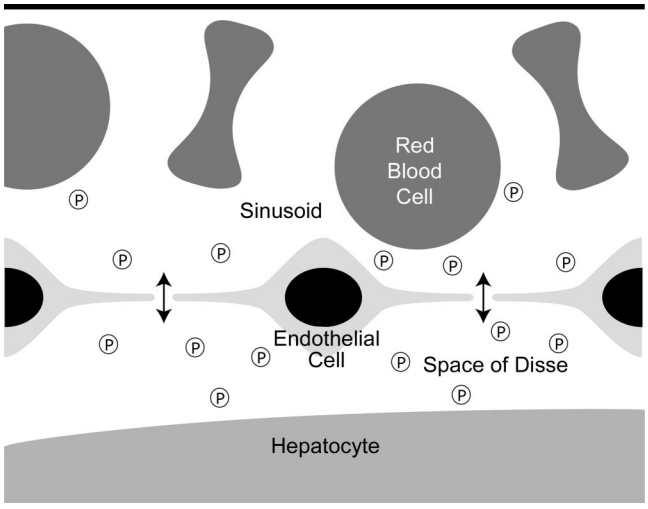


**Figure 2.** Diagram shows microanatomic relationship of red blood cells within sinusoid, fenestrated endothelial cells, plasma *(p)*, space of Disse, and hepatocyte.

in patients with cirrhosis following adenosine-induced hepatic arterial vasodilatation, this arterial reserve has been found to benefit hepatic function and to improve liver oxygenation (33). The hepatic arterial buffer response in cirrhosis has been demonstrated in a rat model (2); supportive data also have been reported in humans with cirrhosis (31,32,34–39). To date, however, a quantitative threshold of change in absolute or fractional arterial flow that delineates the onset of this response and the correlation between flow changes and other markers of cirrhosis have not been determined.

## Development of Primary Liver Malignancy: HCC

Folkman and colleagues (40) first proposed the dependence of sustained tumor growth on angiogenesis in the 1960s, a relationship that continues to be heavily explored today (41,42). In patients with cirrhosis, a spectrum of nodules, including benign regenerative nodules, dysplastic nodules, and HCC, can form; differences in their respective blood supplies can assist in their detection and characterization (43–46). Regenerative nodules, like normal liver parenchyma, continue to receive a majority of their blood supply from the portal vein, whereas the evolution from a low-grade dysplastic nodule to frank HCC is associated with a progression toward increasing arterial blood supply (43–46) (Fig 3). During this evolution, sinusoidal endothelial cells are recruited to create an arteriolar network that gradually replaces normal sinusoidal architecture, and this process is known as "capillarization" (43). At histologic analysis, dysplastic nodules and HCC manifest neoarteriogenesis, which takes the appearance of unpaired or nontriadal arteries, that is, arteries not associated with portal vein branches (43,45,46). Vascular endothelial growth factor expression, a marker of angiogenic activity, has been found to increase linearly and parallels the development of unpaired arteries (47); it is negligible in regenerative nodules, moderate in dysplastic nodules, and strong in HCC (47). Given this progression, serum vascular endothelial growth factor levels in patients with HCC have been explored as markers of tumor activity (48) and as predictors of postoperative tumor recurrence and survival (49).

## Development of Secondary Liver Malignancy: Metastatic Disease

The formation of a metastasis is initiated by the extravasation of a circulating tumor cell within the liver (Fig 3). After tumor enlargement progresses to a point beyond which angiogenesis is necessary to sustain growth, neovascularization occurs in a stepwise fashion (50); proliferation of sinusoidal endothelial cells serves as the primary basis for angiogenesis (50–52). In the peritumoral region, sinusoidal capillarization has been found to occur through a process similar to that seen in hepatocarcinogenesis (50,53). Angiogenesis associated with liver metastases is further assisted by vascular endothelial growth factor expression (53,54). In the presence of metastatic disease, relative increases in hepatic arterial perfusion have been found on a global basis as well (37,38,55–60). The possibility that a tumor-related circulating vasoactive mediator contributes to this global perfusion change has been suggested (61), although further supportive work is necessary.

## Other Physiologic and Iatrogenic Causes of Liver Perfusion Alterations

Although in this review we focus on cirrhosis and malignancy, several other factors may contribute to liver perfusion changes. Of particular note are normal physiologic alterations in blood flow, such as in response to meals (62,63), as well as changes in blood flow that occur as a result of increasingly used minimally invasive tumor therapies, such as radiofrequency ablation, transarterial chemoembolization, and percutaneous ethanol injection (64–75).

An increase in portal venous blood flow is known to occur in postprandial

states as a result of increased splanchnic blood flow; however, this increase is blunted in cirrhosis, an effect thought to be due to increased pressure in the splanchnic venous bed and subsequent portosystemic shunt formation (62,63). The extent to which these opposing changes in flow occur is variable and is difficult to predict. As such, evaluation of global arterial versus portal venous flow to the liver should not be performed in the immediate postprandial state.

Radiofrequency ablation, transcatheter arterial chemoembolization, and percutaneous ethanol injection are increasingly used to treat liver malignancy in a variety of clinical settings (76–78). The enhancement characteristics of tissue after treatment play a major role in the evaluation of treatment success. After tumor treatment, the presence of enhancement at dynamic contrast-enhanced cross-sectional imaging, particularly when seen during the arterial phase, is suggestive of residual or recurrent tumor (64–68,71,72). Peripheral reactive hyperemia, a benign inflammatory response to tissue injury after radiofrequency ablation, however, may manifest as peripheral hyperattenuation during arterial phase imaging. This is usually distinguishable from tumor on the basis of its regular marginal configuration and enhancement characteristics at portal venous phase and equilibrium phase imaging; moreover, this finding typically resolves within 1–4 months (64,65). Also, peripheral wedge-shaped enhancement at arterial phase imaging may be seen as a result of iatrogenic arterial–portal venous shunts from percutaneous therapies (64,65,75). Direct injury to the portal venous system (74) or indirect injury as a result of primary biliary injury (70) can also complicate enhancement patterns. Arterial chemoembolization is known to result in altered hepatic perfusion (69); the degree to which this occurs may depend on the territory of embolized vessels and the extent of subsequent arterial collateral circulation. Perfusion imaging ultimately may have a role in the earlier identification of tumor recurrence if subtle differences in enhancement of benign versus malignant tissue can be captured earlier than they are captured with conventional multiphasic cross-sectional techniques.

## GOALS OF PERFUSION IMAGING

The primary goal of liver perfusion imaging is to increase the sensitivity and specificity with which liver diseases can be identified. The following requirements for optimal perfusion imaging outline a comprehensive approach to this task: *(a)* accurate quantification of arterial and portal venous perfusion on a global and regional basis to evaluate both focal and diffuse abnormalities; *(b)* high spatial resolution to identify perfusion differences in small tumors; *(c)* high temporal resolution to identify kinetic properties of contrast agents that may vary across tumors; *(d)* reliable image-based tracer (contrast agent) concentration measurements to facilitate accurate perfusion quantification; *(e)* robust tracer kinetic modeling methods for accurate derivation of perfusion parameters from enhancement curves, including arterial and portal venous perfusion, mean transit time of the tracer in the liver, and tracer distribution volume, all of which may be abnormal in liver disease; *(f)* whole-liver imaging to enable tumor surveillance; and *(g)* compatibility with existing morphologic imaging techniques to enable all imaging to be performed during a single visit.

In the next section, we review the main approaches to liver perfusion imaging, including scintigraphy, US (with Doppler imaging or transit time interrogation), CT, and MR imaging.

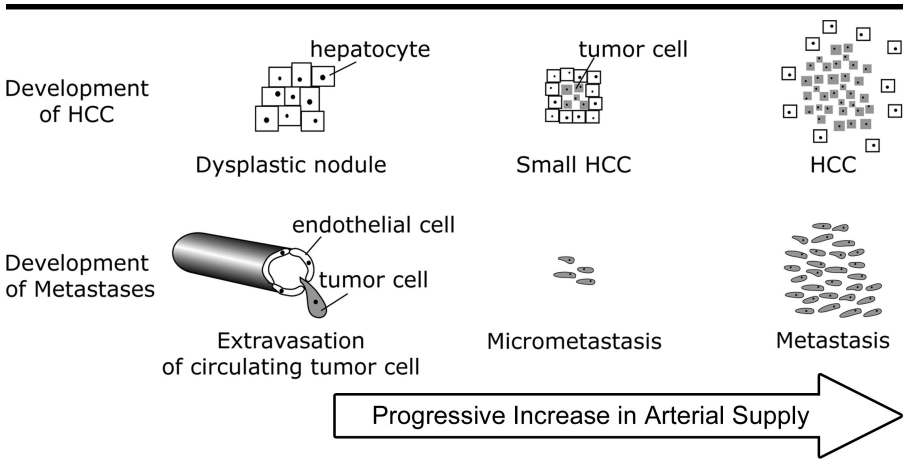


**Figure 3.** Diagram shows physiologic basis of perfusion imaging for tumor surveillance. Progressive increase in arterial versus portal venous supply is associated with both the evolution from a low-grade dysplastic nodule to frank HCC and the development of a metastasis from a circulating tumor cell.

## TECHNIQUES OF LIVER PERFUSION IMAGING

### Perfusion Indices with Scintigraphy

The calculation of liver perfusion indices at flow scintigraphy was initially described in the 1970s and is still used today. In the most commonly described approach, dynamic images are obtained at 1–2-second intervals after the intravenous administration of a radiopharmaceutical agent, such as technetium 99m–labeled tin, sulfur, or albumin colloid or technetium 99m–labeled pertechnetate (35,39,55–57,59,60,79). Liver enhancement is evaluated through a region-of-interest analysis; arterial and portal venous components of liver enhancement are typically distinguished by assuming that peak renal enhancement parallels the onset of the portal venous phase of liver enhancement (35,55–57,59,60,79). By using the slopes of the rise in activity during the arterial phase, designated as $A$, and the portal venous phase, designated as $P$, of liver enhancement, a hepatic arterial perfusion index value is generated and is defined as $A/(A + P)$; this index has been the primary parameter of interest in flow scintigraphy of the liver (35,55–57, 59,60,79).

### Blood Flow Assessment at US

US with Doppler imaging or transit time interrogation enables flow quantification (blood volume divided by time) as opposed to perfusion measurement (blood volume divided by time divided by tissue volume or weight). To calculate flow rates at Doppler US, mean velocity is multiplied by the cross-sectional area of the vessel. Flow measurement with a transit time flowmeter, a technique that necessitates direct placement of a US probe over the blood vessel of interest, is based on measurement of the difference in time that it takes for an ultrasound beam to pass upstream versus the time that it takes for it to pass downstream through flowing blood; this difference is

proportional to blood flow. Three primary approaches to flow measurements in the liver have been described: intraoperative placement of US probes directly over the blood vessels of interest (80,81), intravascular measurements (82,83), and conventional transabdominal imaging (36,84). Invasive approaches are not as feasible in a surveillance setting. By using transabdominal US with Doppler imaging, flow measurements in the hepatic artery (*H*) and portal vein (*PV*) may be readily obtained, and a hepatic Doppler perfusion index value, defined as $H/(H + PV)$, may then be computed (36,84). Two primary disadvantages of Doppler US in the context of perfusion imaging include reported intra- and interobserver variability when the Doppler perfusion index (85,86) is measured and the inability to gain regional parenchymal flow measurements; these may be overcome at CT or MR perfusion imaging.

### Perfusion Assessment with CT

In the early 1990s, Miles et al (37) described liver perfusion imaging at CT by using a dynamic single-section technique in which high-temporal-resolution imaging (3–7 seconds) was performed after rapid intravenous administration of a bolus of iodinated contrast material. Regions of interest were used to generate enhancement curves over the liver, aorta, and spleen (37). Parenchymal enhancement was resolved into arterial and portal venous components by assuming that peak splenic enhancement marked the beginning of dominant portal venous perfusion (37). Hepatic arterial and portal venous perfusion values were calculated by dividing the slopes of the rise in attenuation during the arterial and portal venous phases of liver enhancement, respectively, by peak aortic enhancement (37). A hepatic perfusion index was derived by dividing the calculated arterial perfusion by the sum of arterial and portal perfusion values (37). To better estimate portal perfusion, Blomley et al (38) revised this approach by subtracting arterial phase liver enhancement (modeled after splenic enhancement) from the original liver enhancement curve to derive a "corrected" liver enhancement curve. With this curve, portal venous perfusion was calculated by dividing the slope of the rise in attenuation during the portal phase of liver enhancement by peak portal venous or splenic venous enhancement (38). Calculation of hepatic arterial perfusion was similar to that described by Miles et al (37). These slope-ratio methods of deriving perfusion parameters and indices have dominated the field of CT perfusion imaging (37,38, 58,87).

Two groups have applied tracer kinetic modeling techniques to CT perfusion imaging of the liver (31,88–91). One group (31,88,89) used a dual-input one-compartment model that may be summarized by the following equation:

$$dC_L(t)/dt = k_{1a}C_a(t) + k_{1p}C_p(t) - k_2C_L(t), \quad (1)$$

in which $C_L$, $C_a$, and $C_p$ reflect the tracer (contrast agent) concentration within the liver, hepatic artery, and portal vein, respectively, and $k_{1a}$, $k_{1p}$, and $k_2$ reflect arterial and portal venous inflow and liver outflow constants, respectively. Concentrations of the iodinated contrast agents are determined from attenuation measurements that are based on their known linear relationship (92). Regions of interest placed over the aorta, portal vein, and liver parenchyma are used to generate concentration-time enhancement curves (Fig 4), where the aorta is used as a surrogate for the hepatic artery (31,88,89). A fixed delay time for tracer transit from the aorta to intrahepatic hepatic arterial branches is incorporated; an equal delay time also is used to account for transit from the main portal vein to portal venous branches within the hepatic parenchyma (31,88,89). By fitting measured $C_L(t)$ against predicted values, the rate constants, $k_{1a}$, $k_{1p}$, and $k_2$, can be estimated to yield the best fit and can then be used to calculate hepatic arterial and portal venous perfusion, mean transit time of tracer through the liver, and tracer distribution volume within the liver (31,88,89).

Cuenod et al (90,91) used a deconvolution technique to evaluate CT perfusion imaging of the liver. With this approach, a transfer function (a range of flow values with each value having a different probability) is substituted for each single-valued inflow and outflow rate. These transfer functions are computed by using a linear deconvolution method and then reduced to derive the same perfusion parameters determined by compartmental modeling techniques (including arterial and portal venous perfusion, mean transit time of the tracer through the liver, and tracer distribution volume in the liver).

### Perfusion Assessment with MR Imaging

To date, reports of liver perfusion at MR imaging have been limited and vary considerably. In 1999, Scharf et al (93) reported use of a single-section T1-weighted gradient-echo technique at 1.0 T to perform gadolinium-enhanced perfusion imaging with a 2-second temporal resolution in nine pigs prior to and after partial portal vein occlusion. Intrahepatic thermal diffusion probes were used as the standards of reference for perfusion measurement (93). The relationship between signal intensity and tissue concentration of contrast material was assumed to be linear, and a single-input single-compartment model was used, which prevented delineation of arterial and portal venous contributions (93). The MR imaging–based liver perfusion after partial portal vein occlusion decreased from 117 $mL \cdot min^{-1} \cdot 100\ g^{-1} \pm 42$ (standard deviation) to 48 $mL \cdot min^{-1} \cdot 100\ g^{-1} \pm 22$; thermal diffusion probes measured a decrease in perfusion from an average of 78 $mL \cdot min^{-1} \cdot 100\ g^{-1} \pm 7$ to 47 $mL \cdot min^{-1} \cdot 100\ g^{-1} \pm 15$; a statistically significant correlation was observed between MR imaging–based liver perfusion values and thermal diffusion probe measurements ($P < .01$) (93).

Jackson et al (94) used three-dimensional dynamic contrast-enhanced perfusion MR imaging in humans to investigate lesion-specific permeability mapping. The authors were able to attain 4.1-second temporal resolution by using a $128 \times 128 \times 25$ matrix (94). Contrast material concentration was determined by using a T1 mapping sequence (94). Lesion-specific perfusion parameters were calculated by using a pharmacokinetic model that characterized endothelial permeability and relative blood volume (94). In the input function of the pharmacokinetic model used, only the hepatic arterial supply was considered and the portal vein supply was ignored; therefore, results of evaluation of tissue that received contributions from both the hepatic artery and the portal vein, including normal liver parenchyma, were unreliable.

Materne et al (95) reported single-section high-temporal-resolution liver perfusion imaging in rabbits by using dynamic T1-weighted gradient-echo MR imaging. Tissue tracer concentration was estimated with empiric determination of the relationship between signal intensity and T1 values with the pulse sequence used (95). Region-of-interest analyses over the aorta, portal vein, and liver parenchyma enabled generation of concentration-time curves, which were fitted to a dual-input single-compartment model for liver perfusion (Eq [1]). Arterial and portal inflow and outflow rate constants were determined by

using the model and were used to calculate arterial perfusion (23 $mL \cdot min^{-1} \cdot 100\ mL^{-1} \pm 13$) and portal venous perfusion ($84\ mL \cdot min^{-1} \cdot 100\ mL^{-1} \pm 32$) (95). The distribution volume of contrast material (13% ± 3.7) and the mean transit time (8.9 second ± 4.1) were also calculated. All values correlated well with results obtained by using microspheres (95). This group subsequently used this method of perfusion MR imaging to evaluate perfusion parameters in rabbits with and without cirrhosis (96) and in humans (32), as discussed in detail next in the context of perfusion imaging in cirrhosis.

## PERFUSION IMAGING IN CIRRHOSIS

Relative increases in arterial versus portal venous flow in cirrhosis, as predicted by the hepatic arterial buffer response, have been demonstrated at flow scintigraphy, Doppler US, and CT perfusion imaging (31,35–39). At flow scintigraphy, although hepatic perfusion index values have correlated well with severity of cirrhosis, they have not been shown to be helpful in the prediction of major complications of cirrhosis, such as ascites, variceal rebleeding, and death (35). By using transabdominal Doppler US, Leen et al (36) reported an increase in the hepatic Doppler perfusion index in patients with cirrhosis.

At CT perfusion imaging, Miles et al (37) and Blomley et al (38) reported increased arterial perfusion in patients with cirrhosis. Blomley et al (38) reported a value of 25 $mL \cdot min^{-1} \cdot 100\ mL^{-1}$, and Miles et al (37) reported that of 36 $mL \cdot min^{-1} \cdot 100\ mL^{-1}$; in healthy control groups, Miles et al (37) reported a value of 17 $mL \cdot min^{-1} \cdot 100\ mL^{-1}$, and Blomley et al (38) reported that of 19 $mL \cdot min^{-1} \cdot 100\ mL^{-1}$. These researchers also reported diminished portal perfusion in patients with cirrhosis. Miles et al (37) reported a value of 17 $mL \cdot min^{-1} \cdot 100\ mL^{-1}$, and Blomley et al (38) reported that of 43 $mL \cdot min^{-1} \cdot 100\ mL^{-1}$; in healthy control groups, Miles et al (37) reported a value of 34 $mL \cdot min^{-1} \cdot 100\ mL^{-1}$, and Blomley et al (38) reported that of 93 $mL \cdot min^{-1} \cdot 100\ mL^{-1}$. Calculation of perfusion parameters was based on the slope-ratio methods described by Miles et al (37) and Blomley et al (38).

When Van Beers et al (31) used CT perfusion imaging with dual-input single-compartment modeling (Eq [1]), they found increases in fractional arterial perfusion and mean transit time in a group with cirrhosis (41% ± 27 and 51 second ± 79, respectively), compared with values in healthy controls (17% ± 16 and 16 second ± 5, respectively); however, a

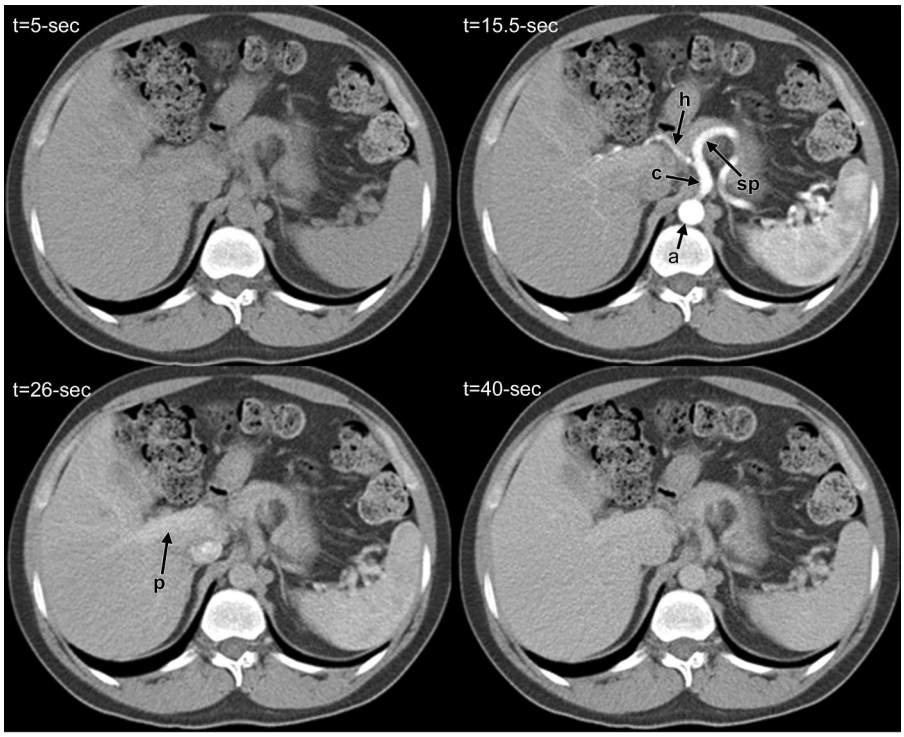


a.

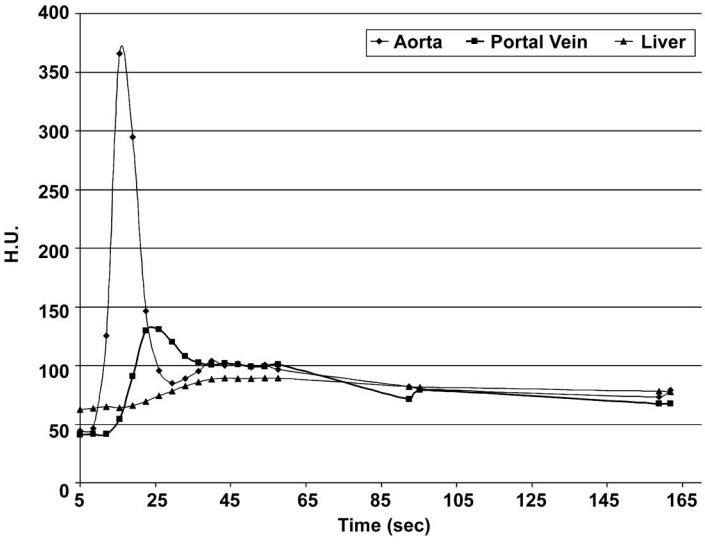


b.

**Figure 4.** CT liver perfusion images and graph that shows enhancement curves. **(a)** Representative transverse CT images (120 kVp, 60 mAs) from four time points in a CT perfusion study performed in a 39-year-old healthy male volunteer (temporal resolution, 3.5 seconds). Rapid sequential single-section imaging was performed after intravenous administration of iodinated contrast material at 9.9 mL/sec by using low-radiation-dose technique. Liver perfusion imaging afforded excellent resolution of arterial ($t$ = 15.5 seconds) and portal venous ($t$ = 26 seconds) phases of imaging. Top right: Arterial phase. Arterial vessels, including aorta *(a)*, celiac trunk *(c)*, hepatic artery *(h)*, and splenic artery *(sp)*, selectively enhanced. Bottom left: Portal venous phase. Selective enhancement of the portal vein *(p)* is seen. **(b)** Graph shows sample enhancement curves derived from analyses of regions of interest placed over aorta, portal vein, and liver. After 57.5 seconds, temporal resolution was decreased substantially to minimize radiation exposure. Use of dual-input single-compartment modeling techniques for derivation of perfusion parameters required enhancement data from both inputs (aorta and portal vein), as well as the liver.

statistically significant difference in distribution volume between the two groups was not observed. Global liver perfusion was lower in the group with cirrhosis (0.67 $mL \cdot min^{-1} \cdot mL^{-1} \pm 0.23$) compared with that in healthy controls (1.08 $mL \cdot min^{-1} \cdot mL^{-1} \pm 0.34$) (31). Increased mean transit time of contrast material through the liver in patients with cirrhosis was attributed to decreased motility of standard contrast materials (low molecular weight) in the extravascular space of Disse because of its collagenization (31). The unchanged distribution volume of contrast material was attributed to continued passage of small molecules into the space of Disse, despite changes of cirrhosis (31).

By using a similar CT perfusion imaging technique with dual-input single-compartment modeling, the same group demonstrated decreased mean transit time and distribution volume with use of a higher-molecular-weight contrast agent compared with a lower-molecular-weight agent in rabbits with hepatic fibrosis (89). These findings were attributed to the progressive restriction of high-molecular-weight molecules to the intravascular space in cirrhosis (89), as previously reported during assessment of the hepatic microcirculation of albumin in rats with cirrhosis (97). This work was followed by use of a perfusion MR imaging technique with dual-input single-compartment modeling in normal rabbits and rabbits with liver fibrosis (96). Van Beers et al (96) reported decreased distribution volume with two high-molecular-weight contrast materials and increased mean transit time for a lower-molecular-weight contrast material in rabbits with liver fibrosis. The clearance of a xenobiotic agent, indocyanine green, correlated with the distribution volume of both high-molecular-weight contrast materials studied, and the collagen content of the liver was inversely related to the distribution volume of the highest-molecular-weight contrast material studied (96). More recently, this group reported increased fractional arterial perfusion and decreased mean transit time when they evaluated humans with cirrhosis by using dual-input single-compartment perfusion MR imaging with a standard low-molecular-weight contrast material (32).

The limited spatial resolution of flow scintigraphy restricts its current applicability. Doppler US is restricted by its reliance on measurements of global flow as opposed to global and regional perfusion. One major limitation of CT perfusion imaging with slope-ratio methods is that the mean transit time and distribution volume of contrast material in the liver, parameters found to be altered in cirrhosis by using compartmental modeling techniques (31,32,89,96), cannot be assessed. Disadvantages of all methods of CT perfusion imaging include the required use of iodinated contrast material and its attendant risks of allergic reactions and nephrotoxicity (98,99), with the latter of major concern in the setting of end-stage cirrhosis because these patients are at risk for hepatorenal syndrome (100), and the radiation doses associated with dynamic CT imaging. The latter will be discussed in detail next in the context of HCC surveillance. Perfusion MR imaging studies, while promising, need to be validated further in humans.

## PERFUSION IMAGING FOR DETECTION OF HCC

To date, true perfusion imaging techniques have not been used for the surveillance of HCC or dysplastic nodules. This is because optimal HCC surveillance necessitates whole-liver perfusion imaging with high spatial resolution to detect and characterize small (<1-cm) lesions. Conventional flow scintigraphic techniques and perfusion positron emission tomographic imaging (101–103) have inadequate spatial resolution for detection of regional perfusion abnormalities. Flow measurements at Doppler US do not enable characterization of regional flow abnormalities.

Whole-liver CT imaging has the potential to provide both high-temporal-resolution and high-spatial-resolution imaging of the entire liver for the detection of HCC; however, the radiation doses must be considered. By using a reduced-dose whole-liver imaging technique (120 kVp, 100 mAs, 5-mm collimation), the radiation dose to the liver with a multi–detector row scanner (Volume Zoom; Siemens, Forchheim, Germany) is approximately 2.8 mSv for a man and 3.4 mSv for a woman for a single scan, as indicated with commercially available software (WinDose; Wellhofer Dosimetry, Schwarzenbruck, Germany). With the assumption that 15–30 3-second whole-liver scans are obtained, the dose equivalent to the liver would be 42–84 mSv for men and 51–102 mSv for women. In comparison, a three-phase liver study performed with 120 kVp and 165 mAs would result in a dose equivalent to the liver of 13.8 mSv for men and 16.8 mSv for women. Thus, a whole-liver CT perfusion study would result in radiation doses that are approximately three to six times greater than those of a routine diagnostic CT examination. A dedicated analysis of the risks versus the benefits of whole-liver CT perfusion imaging may provide greater insight into the significance of this increased dose in the care of specific patient groups.

Perfusion MR imaging represents a promising technique for HCC surveillance. The closest technique to perfusion MR imaging has been use of a double–arterial phase MR imaging technique enabled by a rapid parallel imaging method (termed *sensitivity encoding*, or SENSE); one group reported sensitivity values of 91.7% (33 of 36 lesions) for the detection of HCC and 78.6% (11 of 14 lesions) for the detection of HCC of 1 cm or smaller compared with sensitivity values of 76.3% (29 of 38 lesions) and 27.3% (three of 11 lesions), respectively, by using a protocol that included a single arterial phase (104). These findings suggest the potential of high-temporal-resolution perfusion imaging to improve detection of small HCC.

## PERFUSION IMAGING FOR METASTATIC DISEASE

In patients with known metastatic disease, increased arterial perfusion has been shown by using CT perfusion imaging with the slope-ratio analytic methods described by Miles et al (37) and Blomley et al (38). Blomley et al (38) reported a value of 43 $mL \cdot min^{-1} \cdot 100\ mL^{-1}$, and Miles et al (37) reported that of 50 $mL \cdot min^{-1} \cdot 100\ mL^{-1}$ in patients with known metastatic disease versus values of 19 $mL \cdot min^{-1} \cdot 100\ mL^{-1}$ (38) and 17 $mL \cdot min^{-1} \cdot 100\ mL^{-1}$ (37), respectively, in healthy control groups. Leggett et al (58) also demonstrated increased arterial perfusion (>25 $mL \cdot min^{-1} \cdot 100\ mL^{-1}$) in 82% (nine of 11 patients) of a cohort of patients with overt colorectal metastases examined by using CT perfusion imaging with slope-ratio analytic methods. Similarly, at flow scintigraphy, the relationship between an elevated hepatic perfusion index value and overt metastatic disease has been well established (55–57,59,60). For example, Perkins et al (57) determined a hepatic perfusion index threshold value of 0.37; at values above that level, metastatic disease should be suspected.

The detection of micrometastatic or occult metastatic disease with perfusion imaging has also been studied (56,84,90). By

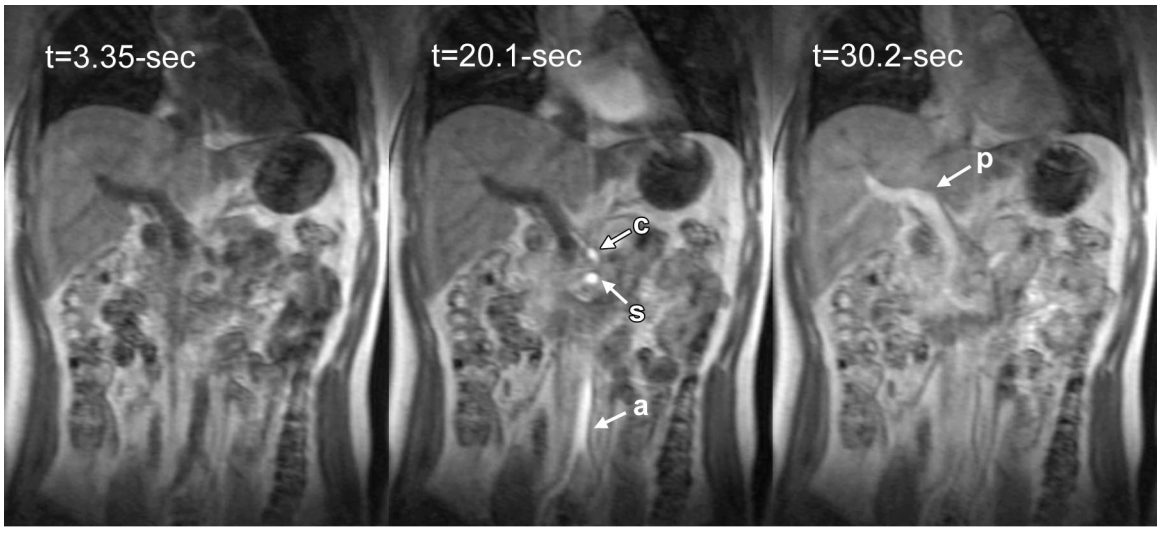


**a.**


**b.**

**Figure 5.** Images demonstrate trade-off between temporal and spatial resolution when whole-liver perfusion MR images and conventional MR images are compared in a healthy 29-year-old woman suspected of having liver hemangioma (not shown). **(a)** Representative images from high-temporal-resolution (3.35 seconds) coronal whole-liver perfusion MR imaging performed with three-dimensional T1-weighted gradient-echo sequence (repetition time msec/echo time msec, 2.3/0.8; 9° flip angle) sequentially at 1.5 T after administration of intravenous contrast material (7 mL at 5 mL/sec, followed by 20-mL normal saline flush). Left: Image obtained immediately after initiation of contrast material injection ($t$ = 3.35 seconds). Middle: Peak arterial enhancement ($t$ = 20.1 seconds). Right: Peak portal venous enhancement ($t$ = 30.2 seconds). Perfusion imaging enables excellent temporal resolution of the arterial and portal venous phases as seen by temporal separation in enhancement of the aorta *(a)* (including celiac trunk *[c]*, superior mesenteric artery *[s]* branches, and portal vein *[p]*). Spatial resolution is suboptimal in that interpolated section thickness is 5.0 mm and voxels (3.1 × 1.8 × 5.0 mm) are anisotropic on images in **a**. **(b)** Representative images obtained from coronal reconstructions from conventional three-dimensional T1-weighted gradient-echo MR images (3.4/1.6, 12° flip angle) obtained after contrast material administration (acquisition time, 22 seconds). Left: Arterial phase. Celiac trunk *(c)*, superior mesenteric artery *(s)*, and portal vein *(p)* are seen. Right: Portal venous phase. Although a timing sequence was performed to achieve temporal resolution of arterial phase, the arterial phase was contaminated by portal venous enhancement. Although temporal resolution was poor, spatial resolution was excellent, with in-plane pixel size of 2.3 × 1.4 mm and interpolated section thickness of 2.0 mm, on images obtained during both phases.

using Doppler US, Leen et al (84) showed that the 5-year survival of patients after potentially curative colon surgery for colorectal carcinoma was 91% in patients with normal hepatic Doppler perfusion index values and 29% in patients with abnormal hepatic Doppler perfusion index values. By using CT perfusion imaging with a deconvolution technique for data analysis, Cuenod et al (90) reported decreased portal perfusion and increased mean transit time in rats with occult liver metastases; arterial perfusion was unchanged. The authors hypothesized that arterial perfusion may be increased in humans with occult metastases secondary to a hepatic arterial buffer response; this response may not have been detectable in rats because of their small baseline arterial contribution to liver perfusion (90).

## FUTURE CHALLENGES OF PERFUSION IMAGING

Improvements in perfusion imaging will stem largely from technical advances. CT perfusion imaging with multi–detector row technology has the potential to provide high-spatial-resolution and high-temporal-resolution whole-liver perfu-

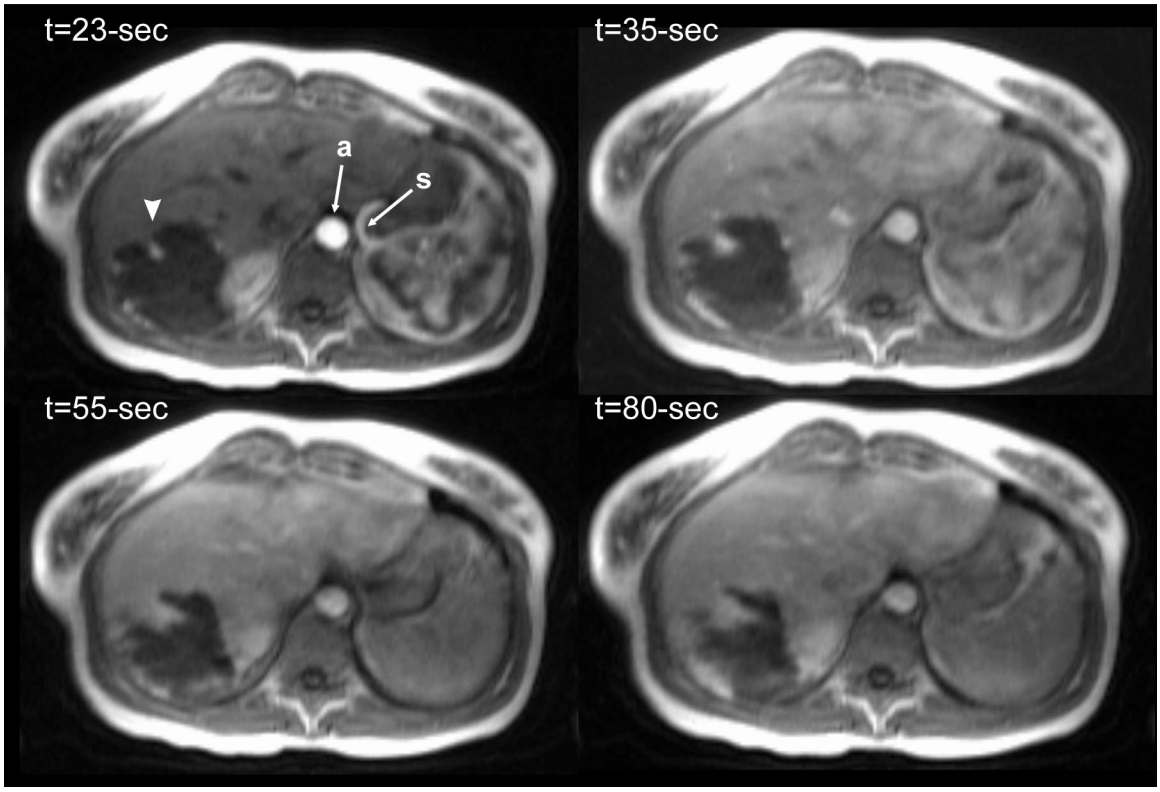


**Figure 6.** Representative images from high-temporal-resolution transverse whole-liver perfusion MR imaging study in a 55-year-old woman with history of hemangioma and metastatic melanoma. For perfusion imaging, three-dimensional T1-weighted gradient-echo whole-liver imaging (2.3/0.8, 9° flip angle) was performed sequentially at 1.5 T with a temporal resolution of 3.22 seconds following the administration of intravenous contrast material (7 mL at 5 mL/sec followed by a 20-mL normal saline flush). This enabled an in-plane spatial resolution of 3.1 × 1.8 mm, with an interpolated section thickness of 5.0 mm. Representative images from four series in the perfusion study are shown. Top left: Arterial phase ($t$ = 23 seconds). Aortic *(a)* and splenic artery *(s)* enhancement are noted. Top right: Early portal venous phase ($t$ = 35 seconds). Bottom left: Late portal venous phase ($t$ = 55 seconds). Bottom right: Delayed phase ($t$ = 80 seconds). A large right lobe lesion (arrowhead) is seen that demonstrates peripheral nodular enhancement with progressive central filling over time, features characteristic of a hemangioma.

sion imaging. Necessary methods for radiation dose reduction are in the early stages of development. Perfusion MR imaging has the potential to enable dynamic whole-liver three-dimensional imaging without the risks of radiation and, therefore, is likely the most promising future approach for perfusion imaging. Effective implementation of perfusion MR imaging, however, requires exploration of optimal techniques for faster higher-resolution whole-liver imaging and subsequent image processing. Moreover, estimation of tissue contrast material concentration at MR imaging needs further work to optimize quantitative perfusion measurements. Finally, validation of existing methods of liver perfusion imaging and perfusion quantification is necessary to determine which techniques are most accurate. The next section focuses on the challenges that are related to perfusion MR imaging at this time.

## Improved Spatial and Temporal Resolution at Perfusion MR Imaging

Strategies that are under development to improve spatial and temporal resolution include improvements in hardware to reduce repetition times, undersampling strategies (105), improved interpolation algorithms, and new parallel imaging methods such as simultaneous acquisition of spatial harmonics (or SMASH) (106) and sensitivity encoding (104), with new coil designs to optimize their implementation. The aim of these strategies should be to obtain volumetric imaging of the liver with isotropic pixels (of approximately 2 mm or less in all three dimensions) in a time frame of 3 seconds or less. We have implemented a fast interpolated three-dimensional gradient-echo technique to perform coronal whole-liver imaging in 3.35 seconds with a pixel size of 3.1 × 1.8 × 5.0 mm (interpolated section thickness) (107) (Fig 5) and transverse whole-liver imaging in 3.22 seconds with a pixel size of 3.1 × 1.8 × 5.0 mm (interpolated section thickness) (Fig 6).

## Quantification of Concentration of Gadolinium-based Contrast Agents

Unlike CT, in MR imaging the relationship between the concentration of gadolinium-based contrast agents and signal intensity is nonlinear and complex. Although this relationship may be nearly linear with specific imaging conditions (primarily related to magnetic field strength, sequences employed, and true tissue concentration of the gadolinium-based agent) (108), more robust techniques for the quantification of gadolinium-based contrast agents have been reported (109,110). One such method used in the context of contrast-enhanced MR imaging of the kidneys relies on the additivity of T1 relaxivity and requires

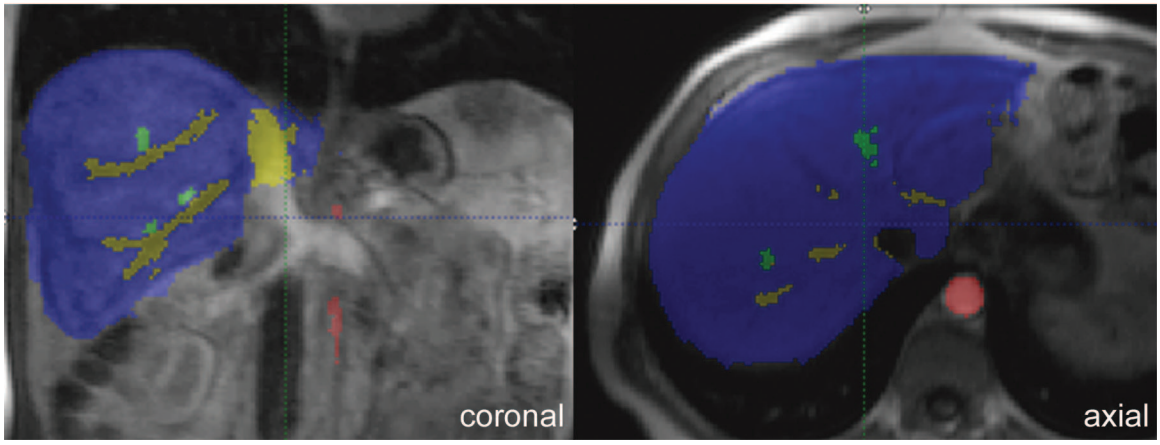


**Figure 7.** Sample color segmentation demonstrated with representative coronal and transverse images from dynamic three-dimensional gradient-echo whole-liver perfusion MR imaging studies (2.3/0.8, 9° flip angle) in a 39-year-old man without cirrhosis (transverse and coronal imaging studies were performed independently). Semiautomated segmentation algorithms enable efficient color-based discrimination of aorta (red), portal vein and its branches (green), liver parenchyma (blue), and hepatic veins and inferior vena cava (dark yellow). Region-of-interest analyses of aortic, portal venous, and liver parenchymal enhancement on the basis of semiautomated segmentation algorithms subsequently can be used for compartmental modeling.

determination of the relationship between signal intensity and T1 relaxation times for a given sequence, as well as the unenhanced T1 values for tissues of interest (109). An alternative and more direct approach relies on T1 mapping for perfusion imaging calculations of the concentrations of gadolinium-based agents (110). These approaches, however, are presently limited to evaluation of a limited number of two-dimensional sections.

### Image Processing

For volumetric CT or perfusion MR imaging of the liver to be clinically useful, automated or semiautomated image processing tools are needed to register multiple three-dimensional data sets and to analyze results in terms of useful clinical parameters, such as arterial perfusion fraction (Fig 7). For the accurate detection of small transient perfusion changes, precise registration of large data sets (on a pixel-by-pixel basis) is critical. Typically, manual drawing of regions of interest requires adjustment to compensate for respiratory motion artifacts. Manual image analysis is not only time-consuming and laborious but also introduces operator-dependent variability. With semiautomated image processing methods, liver perfusion parameters could be calculated with efficiency and perfusion parametric maps could be generated on a pixel-by-pixel basis for the entire liver, as determined with application of tracer kinetic models. Volumetric color-based parametric maps could then facilitate rapid detection of areas of perfusion abnormality; parametric maps already have been demonstrated for single-section CT perfusion imaging (37,87). These tools would facilitate the diagnosis of global and regional abnormalities and the efficient extraction of key parameters of diagnostic importance from large data sets.

### Validation Studies of Quantitative Perfusion Imaging

Validation studies are critical not only for the assessment of methods of data acquisition but also for evaluation of analytic techniques, such as the applicability of dual-input single-compartment modeling to liver perfusion. Moreover, they will help to define the significance of different factors that may contribute to error in perfusion quantification; these factors include parameters such as bolus quality and cardiac function. Computer simulations have been used to estimate the effect of noise on perfusion parameters when compartmental modeling techniques are used (95). In animal studies, radiolabeled microspheres (95) and implantation of thermal diffusion probes (93) have been used for validation of perfusion parameters. To validate perfusion studies in humans, alternative approaches must be developed. In addition, validation of sensitivity for the detection of disease necessitates correlation with whole-liver explant pathology within a short period following imaging. Thin-section pathologic evaluation of the liver can provide an invaluable reference standard in the assessment of diagnostic accuracy for cirrhosis or HCC (13,14).

## CONCLUSION

Perfusion imaging of the liver has the potential to improve detection and characterization of liver disease beyond that enabled by conventional imaging techniques. Preliminary efforts in perfusion imaging are promising; however, several challenges remain. Although technically the most straightforward, clinical implementation of whole-liver CT perfusion imaging requires exploration of methods to reduce radiation exposure. Perfusion MR imaging permits sequential whole-liver imaging without radiation. Techniques that enable improved spatial and temporal resolution and accurate contrast material quantification, however, need to be developed. Future efforts to establish whole-liver perfusion imaging as a clinically feasible and reliable technique may have profound implications for several patient populations. Thus, although perfusion imaging remains in the early stages of development, through continued implementation and exploration of advanced imaging technologies, its clinical value in imaging of the liver should begin to unfold in the near future.

**Acknowledgment:** We gratefully acknowledge the assistance of Martha Helmers, BS, in the creation of the diagrams shown in this review.

**References**


1. Breedis C, Young G. The blood supply of neoplasms in the liver. Am J Pathol 1954; 30:969–977.
2. Richter S, Mucke I, Menger MD, Vollmar B. Impact of intrinsic blood flow regulation in cirrhosis: maintenance of hepatic arterial buffer response. Am J Physiol Gastrointest Liver Physiol 2000; 279: G454–G462.
3. Gulberg V, Haag K, Rossle M, Gerbes AL. Hepatic arterial buffer response in patients with advanced cirrhosis. Hepatology 2002; 35:630–634.
4. Itai Y, Matsui O. Blood flow and liver imaging. Radiology 1997; 202:306–314.
5. Colli A, Fraquelli M, Andreoletti M, Marino B, Zuccoli E, Conte D. Severe liver fibrosis or cirrhosis: accuracy of US for detection—analysis of 300 cases. Radiology 2003; 227:89–94.
6. Di Lelio A, Cestari C, Lomazzi A, Beretta L. Cirrhosis: diagnosis with sonographic study of the liver surface. Radiology 1989; 172:389–392.
7. Hung CH, Lu SN, Wang JH, et al. Correlation between ultrasonographic and pathologic diagnoses of hepatitis B and C virus-related cirrhosis. J Gastroenterol 2003; 38:153–157.
8. Libbrecht L, Bielen D, Verslype C, et al. Focal lesions in cirrhotic explant livers: pathological evaluation and accuracy of pretransplantation imaging examinations. Liver Transpl 2002; 8:749–761.
9. Lim JH, Kim CK, Lee WJ, et al. Detection of hepatocellular carcinomas and dysplastic nodules in cirrhotic livers: accuracy of helical CT in transplant patients. AJR Am J Roentgenol 2000; 175: 693–698.
10. de Ledinghen V, Laharie D, Lecesne R, et al. Detection of nodules in liver cirrhosis: spiral computed tomography or magnetic resonance imaging? a prospective study of 88 nodules in 34 patients. Eur J Gastroenterol Hepatol 2002; 14: 159–165.
11. Peterson MS, Baron RL, Marsh JW Jr, Oliver JH 3rd, Confer SR, Hunt LE. Pretransplantation surveillance for possible hepatocellular carcinoma in patients with cirrhosis: epidemiology and CT-based tumor detection rate in 430 cases with surgical pathologic correlation. Radiology 2000; 217:743–749.
12. Rode A, Bancel B, Douek P, et al. Small nodule detection in cirrhotic livers: evaluation with US, spiral CT, and MRI and correlation with pathologic examination of explanted liver. J Comput Assist Tomogr 2001; 25:327–336.
13. Krinsky GA, Lee VS, Theise ND, et al. Transplantation for hepatocellular carcinoma and cirrhosis: sensitivity of magnetic resonance imaging. Liver Transpl 2002; 8:1156–1164.
14. Krinsky GA, Lee VS, Theise ND, et al. Hepatocellular carcinoma and dysplastic nodules in patients with cirrhosis: prospective diagnosis with MR imaging and explantation correlation. Radiology 2001; 219:445–454.
15. Parkin DM, Bray F, Ferlay J, Pisani P. Estimating the world cancer burden: GLOBOCAN 2000. Int J Cancer 2001; 94:153–156.
16. Barbara L, Benzi G, Gaiani S, et al. Natural history of small untreated hepatocellular carcinoma in cirrhosis: a multivariate analysis of prognostic factors on tumor growth rate and patient survival. Hepatology 1992; 16:132–137.
17. Mazzaferro V, Regalia E, Doci R, et al. Liver transplantation for the treatment of small hepatocellular carcinomas in patients with cirrhosis. N Engl J Med 1996; 334:693–699.
18. Brown RS Jr, Russo MW, Lai M, et al. A survey of liver transplantation from living adult donors in the United States. N Engl J Med 2003; 348:818–825.
19. Ward J, Naik KS, Guthrie JA, Wilson D, Robinson PJ. Hepatic lesion detection: comparison of MR imaging after the administration of superparamagnetic iron oxide with dual-phase CT by using alternative-free response receiver operating characteristic analysis. Radiology 1999; 210:459–466.
20. Valls C, Andia E, Sanchez A, et al. Hepatic metastases from colorectal cancer: preoperative detection and assessment of resectability with helical CT. Radiology 2001; 218:55–60.
21. Valls C, Lopez E, Guma A, et al. Helical CT versus CT arterial portography in the detection of hepatic metastasis of colorectal carcinoma. AJR Am J Roentgenol 1998; 170:1341–1347.
22. Fernando NH, Hurwitz HI. Inhibition of vascular endothelial growth factor in the treatment of colorectal cancer. Semin Oncol 2003; 30:39–50.
23. Rosen LS. Inhibitors of the vascular endothelial growth factor receptor. Hematol Oncol Clin North Am 2002; 16:1173–1187.
24. Lang H, Nussbaum KT, Kaudel P, Fruhauf N, Flemming P, Raab R. Hepatic metastases from leiomyosarcoma: a single-center experience with 34 liver resections during a 15-year period. Ann Surg 2000; 231:500–505.
25. Carlini M, Lonardo MT, Carboni F, et al. Liver metastases from breast cancer: results of surgical resection. Hepatogastroenterology 2002; 49:1597–1601.
26. Elias D, Maisonnette F, Druet-Cabanac M, et al. An attempt to clarify indications for hepatectomy for liver metastases from breast cancer. Am J Surg 2003; 185:158–164.
27. Murata S, Moriya Y, Akasu T, Fujita S, Sugihara K. Resection of both hepatic and pulmonary metastases in patients with colorectal carcinoma. Cancer 1998; 83:1086–1093.
28. Miyazaki M, Itoh H, Nakagawa K, et al. Hepatic resection of liver metastases from gastric carcinoma. Am J Gastroenterol 1997; 92:490–493.
29. Chiandussi L, Greco F, Sardi G, Vaccarino A, Ferraris CM, Curti B. Estimation of hepatic arterial and portal venous blood flow by direct catheterization of the vena porta through the umbilical cord in man: preliminary results. Acta Hepatosplenol 1968; 15:166–171.
30. Schenk WG Jr, McDonald DJ, McDonald DK, Drapanas T. Direct measurement of hepatic blood flow in surgical patients: with related observations on hepatic flow dynamics in experimental animals. Ann Surg 1962; 156:463–471.
31. Van Beers BE, Leconte I, Materne R, Smith AM, Jamart J, Horsmans Y. Hepatic perfusion parameters in chronic liver disease: dynamic CT measurements correlated with disease severity. AJR Am J Roentgenol 2001; 176:667–673.
32. Annet L, Materne R, Danse E, Jamart J, Horsmans Y, Van Beers BE. Hepatic flow parameters measured with MR imaging and Doppler US: correlations with degree of cirrhosis and portal hypertension. Radiology 2003; 229:409–414.
33. Zipprich A, Steudel N, Behrmann C, et al. Functional significance of hepatic arterial flow reserve in patients with cirrhosis. Hepatology 2003; 37:385–392.
34. Koranda P, Myslivecek M, Erban J, Seidlova V, Husak V. Hepatic perfusion changes in patients with cirrhosis indices of hepatic arterial blood flow. Clin Nucl Med 1999; 24:507–510.
35. Bolton RP, Mairiang EO, Parkin A, Ware F, Robinson P, Losowsky MS. Dynamic liver scanning in cirrhosis. Nucl Med Commun 1988; 9:235–247.
36. Leen E, Goldberg JA, Anderson JR, et al. Hepatic perfusion changes in patients with liver metastases: comparison with those patients with cirrhosis. Gut 1993; 34:554–557.
37. Miles KA, Hayball MP, Dixon AK. Functional images of hepatic perfusion obtained with dynamic CT. Radiology 1993; 188:405–411.
38. Blomley MJ, Coulden R, Dawson P, et al. Liver perfusion studied with ultrafast CT. J Comput Assist Tomogr 1995; 19: 424–433.
39. Rypins EB, Fajman W, Sarper R, et al. Radionuclide angiography of the liver and spleen: noninvasive method for assessing the ratio of portal venous to total hepatic blood flow and portasystemic shunt patency. Am J Surg 1981; 142: 574–579.
40. Folkman J, Cole P, Zimmerman S. Tumor behavior in isolated perfused organs: in vitro growth and metastases of biopsy material in rabbit thyroid and canine intestinal segment. Ann Surg 1966; 164:491–502.
41. Folkman J. The role of angiogenesis in tumor growth. Semin Cancer Biol 1992; 3:65–71.
42. Folkman J. Role of angiogenesis in tumor growth and metastasis. Semin Oncol 2002; 29:15–18.
43. Park YN, Yang CP, Fernandez GJ, Cubukcu O, Thung SN, Theise ND. Neoangiogenesis and sinusoidal "capillarization" in dysplastic nodules of the liver. Am J Surg Pathol 1998; 22:656–662.
44. Roncalli M, Roz E, Coggi G, et al. The vascular profile of regenerative and dysplastic nodules of the cirrhotic liver: implications for diagnosis and classification. Hepatology 1999; 30:1174–1178.
45. Krinsky GA, Theise ND, Rofsky NM, Mizrachi H, Tepperman LW, Weinreb JC. Dysplastic nodules in cirrhotic liver: arterial phase enhancement at CT and MR imaging—a case report. Radiology 1998; 209:461–464.
46. Krinsky GA, Zivin SB, Thorner KM, Lee VS, Theise ND, Weinreb JC. Low-grade siderotic dysplastic nodules: determination of premalignant lesions on the basis of vasculature phenotype. Acad Radiol 2002; 9:336–341.

47. Park YN, Kim YB, Yang KM, Park C. Increased expression of vascular endothelial growth factor and angiogenesis in the early stage of multistep hepatocarcinogenesis. Arch Pathol Lab Med 2000; 124:1061–1065.
48. Zhao J, Hu J, Cai J, Yang X, Yang Z. Vascular endothelial growth factor expression in serum of patients with hepatocellular carcinoma. Chin Med J (Engl) 2003; 116:772–776.
49. Chao Y, Li CP, Chau GY, et al. Prognostic significance of vascular endothelial growth factor, basic fibroblast growth factor, and angiogenin in patients with resectable hepatocellular carcinoma after surgery. Ann Surg Oncol 2003; 10: 355–362.
50. Terayama N, Terada T, Nakanuma Y. A morphometric and immunohistochemical study on angiogenesis of human metastatic carcinomas of the liver. Hepatology 1996; 24:816–819.
51. Gervaz P, Scholl B, Mainguene C, Poitry S, Gillet M, Wexner S. Angiogenesis of liver metastases: role of sinusoidal endothelial cells. Dis Colon Rectum 2000; 43: 980–986.
52. Paku S, Lapis K. Morphological aspects of angiogenesis in experimental liver metastases. Am J Pathol 1993; 143:926–936.
53. Terayama N, Terada T, Nakanuma Y. An immunohistochemical study of tumour vessels in metastatic liver cancers and the surrounding liver tissue. Histopathology 1996; 29:37–43.
54. Takeda A, Stoeltzing O, Ahmad SA, et al. Role of angiogenesis in the development and growth of liver metastasis. Ann Surg Oncol 2002; 9:610–616.
55. Leveson SH, Wiggins PA, Nasiru TA, Giles GR, Robinson PJ, Parkin A. Improving the detection of hepatic metastases by the use of dynamic flow scintigraphy. Br J Cancer 1983; 47:719–721.
56. Warren HW, Gallagher H, Hemingway DM, et al. Prospective assessment of the hepatic perfusion index in patients with colorectal cancer. Br J Surg 1998; 85:1708–1712.
57. Perkins AC, Whalley DR, Ballantyne KC, Hardcastle JD. Reliability of the hepatic perfusion index for the detection of liver metastases. Nucl Med Commun 1987; 8:982–989.
58. Leggett DA, Kelley BB, Bunce IH, Miles KA. Colorectal cancer: diagnostic potential of CT measurements of hepatic perfusion and implications for contrast enhancement protocols. Radiology 1997; 205:716–720.
59. Ballantyne KC, Charnley RM, Perkins AC, et al. Hepatic perfusion index in the diagnosis of overt metastatic colorectal cancer. Nucl Med Commun 1990; 11: 23–28.
60. Leveson SH, Wiggins PA, Giles GR, Parkin A, Robinson PJ. Deranged liver blood flow patterns in the detection of liver metastases. Br J Surg 1985; 72:128–130.
61. Carter R, Anderson JH, Cooke TG, Baxter JN, Angerson WJ. Splanchnic blood flow changes in the presence of hepatic tumour: evidence of a humoral mediator. Br J Cancer 1994; 69:1025–1026.
62. Pugliese D, Ohnishi K, Tsunoda T, Sabba C, Albano O. Portal hemodynamics after meal in normal subjects and in patients with chronic liver disease studied by echo-Doppler flowmeter. Am J Gastroenterol 1987; 82:1052–1056.
63. Gaiani S, Bolondi L, Li Bassi S, Santi V, Zironi G, Barbara L. Effect of meal on portal hemodynamics in healthy humans and in patients with chronic liver disease. Hepatology 1989; 9:815–819.
64. Lim HK, Choi D, Lee WJ, et al. Hepatocellular carcinoma treated with percutaneous radio-frequency ablation: evaluation with follow-up multiphase helical CT. Radiology 2001; 221:447–454.
65. Dromain C, de Baere T, Elias D, et al. Hepatic tumors treated with percutaneous radio-frequency ablation: CT and MR imaging follow-up. Radiology 2002; 223:255–262.
66. Katyal S, Oliver JH, Peterson MS, Chang PJ, Baron RL, Carr BI. Prognostic significance of arterial phase CT for prediction of response to transcatheter arterial chemoembolization in unresectable hepatocellular carcinoma: a retrospective analysis. AJR Am J Roentgenol 2000; 175:1665–1672.
67. Kim HC, Kim AY, Han JK, et al. Hepatic arterial and portal venous phase helical CT in patients treated with transcatheter arterial chemoembolization for hepatocellular carcinoma: added value of unenhanced images. Radiology 2002; 225: 773–780.
68. Kubota K, Hisa N, Nishikawa T, et al. Evaluation of hepatocellular carcinoma after treatment with transcatheter arterial chemoembolization: comparison of Lipiodol-CT, power Doppler sonography, and dynamic MRI. Abdom Imaging 2001; 26:184–190.
69. Makita O, Yamashita Y, Arakawa A, et al. Diffuse perfusion abnormality of the liver parenchyma on angiography-assisted helical CT in relation to cirrhosis and previous treatments: a potential diagnostic pitfall for detecting hepatocellular carcinoma. Clin Imaging 2000; 24: 292–297.
70. Yu JS, Kim KW, Park MS, Yoon SW. Bile duct injuries leading to portal vein obliteration after transcatheter arterial chemoembolization in the liver: CT findings and initial observations. Radiology 2001; 221:429–436.
71. Bartolozzi C, Lencioni R, Caramella D, Falaschi F, Cioni R, DiCoscio G. Hepatocellular carcinoma: CT and MR features after transcatheter arterial embolization and percutaneous ethanol injection. Radiology 1994; 191:123–128.
72. Bartolozzi C, Lencioni R, Caramella D, Mazzeo S, Ciancia EM. Treatment of hepatocellular carcinoma with percutaneous ethanol injection: evaluation with contrast-enhanced MR imaging. AJR Am J Roentgenol 1994; 162:827–831.
73. Bartolozzi C, Crocetti L, Cioni D, Donati FM, Lencioni R. Assessment of therapeutic effect of liver tumor ablation procedures. Hepatogastroenterology 2001; 48: 352–358.
74. Yoshikawa J, Matsui O, Kadoya M, et al. Hepatocellular carcinoma: CT appearance of parenchymal changes after percutaneous ethanol injection therapy. Radiology 1995; 194:107–111.
75. Yu JS, Kim KW, Jeong MG, Lee JT, Yoo HS. Nontumorous hepatic arterial-portal venous shunts: MR imaging findings. Radiology 2000; 217:750–756.
76. Livraghi T. Radiofrequency ablation, PEIT, and TACE for hepatocellular carcinoma. J Hepatobiliary Pancreat Surg 2003; 10:67–76.
77. Livraghi T, Solbiati L, Meloni F, Ierace T, Goldberg SN, Gazelle GS. Percutaneous radiofrequency ablation of liver metastases in potential candidates for resection: the "test-of-time approach." Cancer 2003; 97:3027–3035.
78. Camma C, Schepis F, Orlando A, et al. Transarterial chemoembolization for unresectable hepatocellular carcinoma: meta-analysis of randomized controlled trials. Radiology 2002; 224:47–54.
79. Parkin A, Robinson PJ, Baxter P, Leveson SH, Wiggins PA, Giles GR. Liver perfusion scintigraphy: method, normal range and laparotomy correlation in 100 patients. Nucl Med Commun 1983; 4:395–402.
80. Doi R, Inoue K, Kogire M, et al. Simultaneous measurement of hepatic arterial and portal venous flows by transit time ultrasonic volume flowmetry. Surg Gynecol Obstet 1988; 167:65–69.
81. Jakab F, Rath Z, Schmal F, Nagy P, Faller J. Changes in hepatic hemodynamics due to primary liver tumours. HPB Surg 1996; 9:245–248.
82. Kleber G, Steudel N, Behrmann C, et al. Hepatic arterial flow volume and reserve in patients with cirrhosis: use of intra-arterial Doppler and adenosine infusion. Gastroenterology 1999; 116:906–914.
83. Hubner GH, Steudel N, Kleber G, Behrmann C, Lotterer E, Fleig WE. Hepatic arterial blood flow velocities: assessment by transcutaneous and intravascular Doppler sonography. J Hepatol 2000; 32:893–899.
84. Leen E, Goldberg JA, Angerson WJ, McArdle CS. Potential role of Doppler perfusion index in selection of patients with colorectal cancer for adjuvant chemotherapy. Lancet 2000; 355:34–37.
85. Oppo K, Leen E, Angerson WJ, Cooke TG, McArdle CS. Doppler perfusion index: an interobserver and intraobserver reproducibility study. Radiology 1998; 208:453–457.
86. Fowler RC, Harris KM, Swift SE, Ward M, Greenwood DC. Hepatic Doppler perfusion index: measurement in nine healthy volunteers. Radiology 1998; 209:867–871.
87. Dugdale PE, Miles KA. Hepatic metastases: the value of quantitative assessment of contrast enhancement on computed tomography. Eur J Radiol 1999; 30:206–213.
88. Materne R, Van Beers BE, Smith AM, et al. Non-invasive quantification of liver perfusion with dynamic computed tomography and a dual-input one-compartmental model. Clin Sci (Lond) 2000; 99:517–525.
89. Materne R, Annet L, Dechambre S, et al. Dynamic computed tomography with low- and high-molecular-mass contrast agents to assess microvascular permeability modifications in a model of liver fibrosis. Clin Sci (Lond) 2002; 103:213–216.

90. Cuenod C, Leconte I, Siauve N, et al. Early changes in liver perfusion caused by occult metastases in rats: detection with quantitative CT. Radiology 2001; 218:556–561.
91. Cuenod CA, Leconte I, Siauve N, et al. Deconvolution technique for measuring tissue perfusion by dynamic CT: application to normal and metastatic liver. Acad Radiol 2002; 9(suppl 1):S205–S211.
92. Axel L. Cerebral blood flow determination by rapid-sequence computed tomography: theoretical analysis. Radiology 1980; 137:679–686.
93. Scharf J, Zapletal C, Hess T, et al. Assessment of hepatic perfusion in pigs by pharmacokinetic analysis of dynamic MR images. J Magn Reson Imaging 1999; 9:568–572.
94. Jackson A, Haroon H, Zhu XP, Li KL, Thacker NA, Jayson G. Breath-hold perfusion and permeability mapping of hepatic malignancies using magnetic resonance imaging and a first-pass leakage profile model. NMR Biomed 2002; 15: 164–173.
95. Materne R, Smith AM, Peeters F, et al. Assessment of hepatic perfusion parameters with dynamic MRI. Magn Reson Med 2002; 47:135–142.
96. Van Beers BE, Materne R, Annet L, et al. Capillarization of the sinusoids in liver fibrosis: noninvasive assessment with contrast-enhanced MRI in the rabbit. Magn Reson Med 2003; 49:692–699.
97. Varin F, Huet PM. Hepatic microcirculation in the perfused cirrhotic rat liver. J Clin Invest 1985; 76:1904–1912.
98. Katayama H, Yamaguchi K, Kozuka T, Takashima T, Seez P, Matsuura K. Adverse reactions to ionic and nonionic contrast media: a report from the Japanese Committee on the Safety of Contrast Media. Radiology 1990; 175:621–628.
99. Prince MR, Arnoldus C, Frisoli JK. Nephrotoxicity of high-dose gadolinium compared with iodinated contrast. J Magn Reson Imaging 1996; 6:162–166.
100. Moreau R. Hepatorenal syndrome in patients with cirrhosis. J Gastroenterol Hepatol 2002; 17:739–747.
101. Taniguchi H, Oguro A, Koyama H, Masuyama M, Takahashi T. Analysis of models for quantification of arterial and portal blood flow in the human liver using PET. J Comput Assist Tomogr 1996; 20:135–144.
102. Taniguchi H, Oguro A, Takeuchi K, et al. Difference in regional hepatic blood flow in liver segments: non-invasive measurement of regional hepatic arterial and portal blood flow in human by positron emission tomography with H2(15)O. Ann Nucl Med 1993; 7:141–145.
103. Yamaguchi A, Taniguchi H, Kunishima S, Koh T, Yamagishi H. Correlation between angiographically assessed vascularity and blood flow in hepatic metastases in patients with colorectal carcinoma. Cancer 2000; 89:1236–1244.
104. Yoshioka H, Takahashi N, Yamaguchi M, Lou D, Saida Y, Itai Y. Double arterial phase dynamic MRI with sensitivity encoding (SENSE) for hypervascular hepatocellular carcinomas. J Magn Reson Imaging 2002; 16:259–266.
105. Barger AV, Block WF, Toropov Y, Grist TM, Mistretta CA. Time-resolved contrast-enhanced imaging with isotropic resolution and broad coverage using an undersampled 3D projection trajectory. Magn Reson Med 2002; 48:297–305.
106. Sodickson DK, McKenzie CA, Ohliger MA, Yeh EN, Price MD. Recent advances in image reconstruction, coil sensitivity calibration, and coil array design for SMASH and generalized parallel MRI. MAGMA 2002; 13:158–163.
107. Pandharipande PV, Krinsky GA, Rusinek H, Lee VS. Perfusion imaging of the liver with time-resolved, contrast-enhanced, whole-liver MRI (abstr). In: Proceedings of the 11th Meeting of the International Society for Magnetic Resonance in Medicine. Berkeley, Calif: International Society for Magnetic Resonance in Medicine, 2003; 1251.
108. Takeda M, Katayama Y, Tsutsui T, Komeyama T, Mizusawa T. Does gadolinium-diethylene triamine pentaacetic acid enhanced MRI of kidney represent tissue concentration of contrast media in the kidney? in vivo and in vitro study. Magn Reson Imaging 1994; 12:421–427.
109. Rusinek H, Lee VS, Johnson G. Optimal dose of Gd-DTPA in dynamic MR studies. Magn Reson Med 2001; 46:312–316.
110. McKenzie CA, Prato FS, Thornhill RE, Drost DJ. T(1) fast acquisition relaxation mapping (T[1]-FARM): optimized data acquisition. Magn Reson Imaging 2000; 18:129–138.